Distributed Real-time Optimal Power Flow Strategy for DC Microgrid Under Stochastic Communication Networks

Jian Hu and Hao Ma

***Abstract*—This paper addresses a distributed real-time optimal power flow (RTOPF) strategy for DC microgrids. In this paper, we focus on the scenarios where local information sharing is conducted in stochastic communication networks subject to random failures. Most existing real-time optimal power flow (OPF) algorithms for the DC microgrid require all controllers to work in concert with a fixed network topology to maintain a zero gap between estimated global constraint violations. Thus, the high reliability of communication is required to ensure their convergence. To address this issue, the proposed RTOPF strategy tolerates stochastic communication failures and can seek the optimum with a constant step size considering the operation limitations of the microgrid. These aspects make the strategy suitable for real-time optimization, particularly when the communication is not reliable. In addition, this strategy does not require information from non-dispatchable devices, thereby reducing the number of sensors and controllers in the system. The convergence of the proposed strategy and the optimal equilibrium points are theoretically proven. Finally, simulations of a 30-bus DC microgrid are performed to validate the effectiveness of the proposed designs.**

***Index Terms*—DC microgrid, distributed optimization, stochastic communication network, consensus algorithm.**

I. Introduction

MICROGRIDS are generally categorized into AC and DC systems. The DC microgrids are more friendly to some devices such as photovoltaic (PV) panels, batteries, and electric vehicles because they are inherently DC devices. Thus, the DC microgrids can reduce the conversion process, which improves the efficiency and reliability. In addition, the DC microgrids are free of frequency regulation, reactive power control, or AC related power quality problems [1], which results in less complex control systems. The hierarchical control is frequently utilized in DC microgrids [2], [3]. The most popular solution of the primary control is droop control [4], where load sharing is mainly determined by the droop coefficient. The secondary control is utilized to eliminate the voltage deviation and achieve perfect power sharing through centralized [5] or distributed [6], [7] methods. The tertiary control aims to achieve the optimal operation point by controlling the power flow among distribution systems [8]. Traditionally, the secondary control and tertiary control are implemented in a centralized manner [9]. However, these solutions encounter considerable challenges in large systems, including single-point failures, heavy communication burden, and slow dynamic processes [10]. Therefore, self-organizing distributed approaches, where no control center is required, have recently been used to develop scalable and robust algorithms [11]-[13].

Several algorithms combining real-time coordination and steady-state optimization are developed for both AC systems [14], [15] and DC systems [16]-[22] to enhance the system performances. These studies are inspiring because they can achieve optimal power flow (OPF) in real-time scenarios. In [16] and [17], the OPF condition is reached by utilizing consensus algorithms to ensure the incremental costs of different converters to be identical. In [18], a sub-gradient method is combined with a consensus approach to enhance the convergence performance of the system. In [19], the OPF problem of a stand-alone DC microgrid is formulated as an exact second-order cone program and solved through the primal-dual decomposition in a distributed manner. In [21], the generation cost minimization and individual bus voltage regulation are obtained in a DC microgrid using a consensus algorithm. In [22] and [23], an event-trigger control algorithm is utilized to reduce the communication burden of the system. However, [23] focuses on the current sharing and voltage regulation, and it cannot achieve the OPF condition.

However, the aforementioned algorithms assume that the communication is ideal, which is not always true. They are vulnerable to some random failures that result in time-varying communication topologies. In addition, the convergence and accuracy of these algorithms would be affected by non-ideal communication, as they require static network topologies. To the best of our knowledge, only a few studies have been devoted to the online optimization of DC microgrids with non-ideal communication. The effects of communication delay are considered in [24] and [25]. In [26], the economic power dispatch (EPD) problem is discussed through a

Manuscript received: October 29, 2021; revised: March 30, 2022; accepted: July 5, 2022. Date of CrossCheck: July 5, 2022. Date of online publication: August 18, 2022.

This article is distributed under the terms of the Creative Commons Attribution 4.0 International License (http://creativecommons.org/licenses/by/4.0/).

J. Hu (corresponding author) is with Power Dispatching Control Center, Nanjing Power Supply Company, State Grid Corporation of China, Nanjing 210019, China (e-mail: hujian_000999@163.com).

H. Ma is with School of Electrical Engineering, Zhejiang University, Hangzhou, China (e-mail: mahao@zju.edu.cn).

DOI: 10.35833/MPCE.2021.000730

dynamic communication topology. However, this requires the step size of the system to be diminished, which limits its application in real-time control. Reference [27] solves the EPD problem under uncertainties but its results are limited to static communication topologies, making it inapplicable to time-varying communication topologies. In [28], the package loss of communication is considered and analyzed. In [29], the EPD problem is solved using a gossip algorithm. However, only one communication link can transmit information at each iteration, which limits the convergence speed of the algorithm.

After a careful review of recent literature, we found that the studies that focus on online operations have not considered the communication failures [16]-[23]. In fact, online algorithms are more sensitive to the communication failures because retransmission is complicated, and this process substantially increases the transmission time. Besides, algorithms that consider the communication failures [26] - [29] have their own limitations. First, these algorithms need to iterate on all variables in the cyber layer until the convergence is reached before the solution is applied to the power system. In general, intermediate results do not satisfy the power flow equations or operation constraints. As a result, these algorithms cannot be directly applied to real-time systems. Second, these algorithms require information from all devices including non-dispatchable devices, e.g., fixed loads, PV panels, and wind turbines, which are not always practical or economical, as the number of non-dispatchable devices is much greater than that of dispatchable ones.

The proposed algorithm is a real-time OPF strategy for DC microgrids, which can work under stochastic communication networks. It is particularly suitable for scenarios where the online optimization is required and the communication topology is time-varying. The proposed algorithm tracks the bus voltage and the current injection of a dispatchable device to calculate their references under a non-ideal communication network. It tends to be robust under uncertainties and disturbances due to the fluctuating loads and volatile renewables. In addition, the proposed algorithm can operate in communication networks with random failures and stochastic topologies, which greatly enhances its reliability in real-time scenarios. Furthermore, the communication with non-dispatchable devices, e.g., fixed loads and renewable energy resources, is not required, as this information can be obtained by local measurement using dispatchable devices. The convergence and optimality of the proposed algorithm are proven in this paper.

The main contributions of this paper are listed as follows.

1) The proposed algorithm can work in communication networks with random failures and stochastic topologies, and its utility can be enhanced when the communication is less reliable. This is a distinctive feature, which is not observed in most existing real-time algorithms.

2) The proposed algorithm can work under dynamic communications, which further enhances its reliability.

3) The proposed algorithm is fully distributed, and only the communications with neighbors are needed. In addition, the information of non-dispatchable devices such as PV or fixed loads is not required. These aspects significantly reduce the number of sensors and controllers.

The remainder of this paper is organized as follows. In Section II, we formulate the model of stochastic communication network and OPF problem. Section III introduces the proposed RTOPF strategy. In Section IV, case studies are presented to verify the accuracy, dynamic performance, robustness to communication failure and delay, and the plug-and-play features of the proposed algorithm. Finally, the conclusion and future work are given in Section V.

II. Model of Stochastic Communication Network and OPF Problem

A. Model of Stochastic Communication Network

The communications between controllers may be unreliable due to errors or failures. In this study, controllers communicate with each other through a stochastic communication network described by graph $\mathcal{G}=(\mathcal{V},\mathcal{E})$, where each vertex $i\in\mathcal{V}$ denotes a controller; each edge $e_{ij}\in\mathcal{E}$ denotes a communication link with positive weight w_{ij}; N is the number of elements in $\mathcal{V}$; and $\mathcal{N}_i=\{j|e_{ij}\in\mathcal{E}\}$ denotes the neighbors of controller i. In the proposed algorithm, the random communication failures are considered. At each time interval of the algorithm, the communication link e_{ij} is active or inactive with probability p_{ij} or $1-p_{ij}$. The weight matrix $\boldsymbol{W}_k$ is used to define the behavior of communication at time interval k, whose element $w_{ij}(k)$ is expressed as:

$$w_{ij}(k)=\begin{cases} l_{ij} & (i,j)\in\mathcal{R}(k) \\ 0 & (i,j)\notin\mathcal{R}(k) \\ 1-\sum_{i\neq j}w_{ij}(k) & i=j \end{cases} \tag{1}$$

where $\mathcal{R}(k)$ is the set of active communication links at time interval k; and l_{ij} is the communication weight between two nodes.

In this paper, the following assumption on $\boldsymbol{W}_k$ is made.

Assumption 1: the weight matrix $\boldsymbol{W}_k$ is drawn independent identically distributed (i.i.d) from probability space $\mathcal{F}$ such that each $\boldsymbol{W}_k$ fulfills (2) and (3).

$$\begin{cases} \mathbf{1}^{\mathrm{T}}\boldsymbol{W}_k=\mathbf{1}^{\mathrm{T}} \\ \boldsymbol{W}_k\mathbf{1}=\mathbf{1} \end{cases} \tag{2}$$

$$0<\rho(E(\boldsymbol{W}_k{}^{\mathrm{T}}\boldsymbol{W}_k-\boldsymbol{J}))<1 \tag{3}$$

where $\mathbf{1}$ is the vector containing all ones; and $\boldsymbol{J}=\mathbf{1}\mathbf{1}^{\mathrm{T}}/N$ represents the average matrix, which ensures that all elements of a vector are equal to their average value; and $\rho(\cdot)$ and $E(\cdot)$ are the spectral radius and expected value, respectively.

Remark 1: this assumption can be easily fulfilled by appropriate tuning of l_{ij}. Equation (2) will hold if the two-way communication is utilized, which means $l_{ij}=l_{ji}$. Equation (3) will hold if $l_{ij}=1/(\max(N_i)+1)$, where N_i is the number of elements in $\mathcal{N}_i$.

B. OPF Problem Formulation

Two main objectives need to be addressed with respect to a DC microgrid. One is how to efficiently dispatch the ener-

gy from distributed generators (DGs) to meet the demands of all loads economically. The other one is to maintain desirable voltage profiles. Considering a DC microgrid consisting of N DGs, to accommodate the two objectives, a multi-objective optimization goal is set as:

$$\min_{v_i, i_i} J = \alpha \sum_{i=1}^{N} (a_i P_i^2 + b_i P_i + c_i) + \beta \sum_{i=1}^{N} (v_i - v_{nom})^2 \tag{4}$$

$$P_i = v_i i_i \tag{5}$$

where a_i, b_i, and c_i are the generation cost coefficients; v_i and i_i are the bus voltage and current injection, respectively; P_i is the power output of each bus; v_{nom} is the nominal voltage of the system; and the positive parameters α and β are the trade-off weight coefficients balancing the two objectives. In practice, these parameters are selected based on the specific requirements. If the cost is more important, α would be increased. The result is that more emphasis would be placed on the economic aspects of the solution. By contrast, β would be increased if the voltage deviation is more important.

Because of the existence of the bi-linear term (5), the original problem in (4) and (5) is non-convex and it cannot be efficiently solved [30]. Notice that the voltage of the converter is strictly limited by operation limitations, and the voltage deviation can be ignored when calculating P_i [16], [21], [31]. Combining (4) and (5) by replacing v_i with v_{nom} yields a simplified convex problem as:

$$\min_{v_i, i_i} J = \alpha \sum_{i=1}^{N} (a_i' i_i^2 + b_i' i_i + c_i) + \beta \sum_{i=1}^{N} (v_i - v_{nom})^2 \tag{6}$$

where $a_i' = a_i v_{nom}^2$ and $b_i' = b_i v_{nom}$. Based on Ohm's law, the bus voltage and current injections are related to the conductance matrix:

$$\begin{bmatrix} \boldsymbol{I} \\ \boldsymbol{I}_F \end{bmatrix} = \begin{bmatrix} \boldsymbol{G}_{DD} & \boldsymbol{G}_{DF} \\ \boldsymbol{G}_{FD} & \boldsymbol{G}_{FF} \end{bmatrix} \begin{bmatrix} \boldsymbol{V} \\ \boldsymbol{V}_F \end{bmatrix} \tag{7}$$

where $\boldsymbol{V}$, $\boldsymbol{V}_F$ and $\boldsymbol{I}$, $\boldsymbol{I}_F$ are the vectors of the bus voltages and current injections connected to dispatchable and non-dispatchable devices, respectively; and $\boldsymbol{G}_{DD}$, $\boldsymbol{G}_{DF}$, $\boldsymbol{G}_{FD}$, and $\boldsymbol{G}_{FF}$ are the conductance matrices that represent the relationships between bus voltages and current outputs. Then, $\boldsymbol{I}$ is solved as:

$$\boldsymbol{I} = (\boldsymbol{G}_{DD} - \boldsymbol{G}_{DF}\boldsymbol{G}_{FF}^{-1}\boldsymbol{G}_{FD})\boldsymbol{V} + \boldsymbol{G}_{DF}\boldsymbol{G}_{FF}^{-1}\boldsymbol{I}_F \tag{8}$$

Three constraints in (9)-(11) are considered in the operation. Formulas (9) and (10) are the voltage and current constraints, and (11) represents the physical limitation of the real-time operation.

$$\underline{v} \le v_i \le \bar{v} \qquad i = 1, 2, ..., N \tag{9}$$

$$\underline{i}_i \le i_i \le \bar{i}_i \qquad i = 1, 2, ..., N \tag{10}$$

$$\boldsymbol{I} = \boldsymbol{G}\boldsymbol{V} + \boldsymbol{F} \tag{11}$$

where $\underline{v}$, $\bar{v}$ and $\underline{i}_i$, $\bar{i}_i$ are the lower and upper bounds of the bus voltage and current injection, respectively; and $\boldsymbol{G} = \boldsymbol{G}_{DD} - \boldsymbol{G}_{DF}\boldsymbol{G}_{FF}^{-1}\boldsymbol{G}_{FD}$ and $\boldsymbol{F} = \boldsymbol{G}_{DF}\boldsymbol{G}_{FF}^{-1}\boldsymbol{I}_F$ are the constant matrices determined by conductance matrices and non-dispatchable devices, respectively.

An assumption is made regarding the OPF problem:

Assumption 2 (Slater's condition): $\boldsymbol{V}$ and $\boldsymbol{I}$ exist such that constraints (9)-(11) hold [32]. In other words, the OPF problem is feasible.

III. RTOPF Strategy

The proposed algorithm has a hierarchical structure, as shown in Fig. 1.

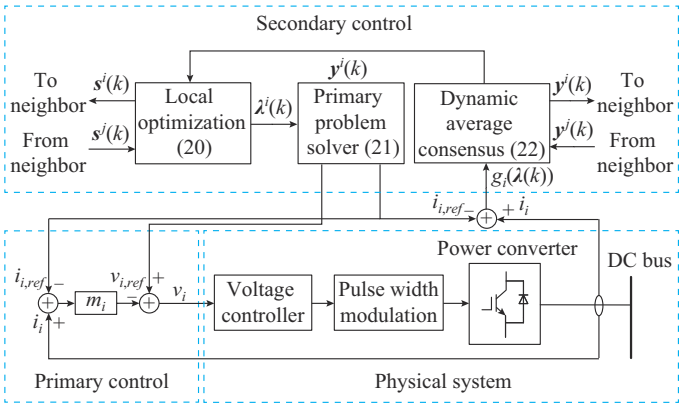

Fig. 1. Control diagram of proposed algorithm.

The primary control level uses droop control to maintain the power balance of the system:

$$v_i = v_{i,ref} - m_i(i_i - i_{i,ref}) \quad i = 1, 2, ..., N \tag{12}$$

where $v_{i,ref}$ and $i_{i,ref}$ are the reference bus voltage and current injection, respectively; and m_i is the droop coefficient. No communication is required at this level. Thus, the power balance of the system can be obtained in real time. The goal of the secondary control is to solve the constrained optimization problem in a distributed manner to determine the reference values $v_{i,ref}$ and $i_{i,ref}$. The voltage vector $\boldsymbol{V}$ and current vector $\boldsymbol{I}$ fulfill the operation relationship in (11), because they are real-time physical values measured by the controllers.

Combining (11) and (12) yields:

$$\boldsymbol{I} = \boldsymbol{A}\boldsymbol{V}_{ref} + \boldsymbol{B}\boldsymbol{I}_{ref} + \boldsymbol{C} \tag{13}$$

where $\boldsymbol{V}_{ref}$ and $\boldsymbol{I}_{ref}$ are the vectors of reference voltage and current, respectively; and $\boldsymbol{A} = (\boldsymbol{E} + \boldsymbol{G}\boldsymbol{M})^{-1}\boldsymbol{G}$, $\boldsymbol{B} = (\boldsymbol{E} + \boldsymbol{G}\boldsymbol{M})^{-1}\boldsymbol{G}\boldsymbol{M}$, and $\boldsymbol{C} = (\boldsymbol{E} + \boldsymbol{G}\boldsymbol{M})^{-1}\boldsymbol{F}$ are the constant matrices determined by system parameters, $\boldsymbol{M} = \mathrm{diag}\{m_i\}$, and $\boldsymbol{E}$ is the N-order identity matrix.

Note that if $i_{i,ref} = i_i$, we have $v_i = v_{i,ref}$ based on (13). Therefore, (11) can be replaced with (14).

$$\boldsymbol{I} = \boldsymbol{I}_{ref} \tag{14}$$

The dual method [33] is applied to develop a distributed iterative approach, in which $v_{i,ref}$ and $i_{i,ref}$ are moved in the direction of minimizing the dual function. The dual function $\phi(\boldsymbol{\lambda})$ is defined as:

$$\phi(\boldsymbol{\lambda}) = \inf_{\boldsymbol{V}_{ref} \in \mathbb{V}, \boldsymbol{I}_{ref} \in \mathbb{I}} L(\boldsymbol{V}_{ref}, \boldsymbol{I}_{ref}, \boldsymbol{\lambda}) = \inf_{\boldsymbol{V}_{ref} \in \mathbb{V}, \boldsymbol{I}_{ref} \in \mathbb{I}} \left\{ J(\boldsymbol{V}_{ref}, \boldsymbol{I}_{ref}) + \sum_{i=1}^{N} (\boldsymbol{\lambda}^i)^{\mathrm{T}} \cdot \left[\boldsymbol{A}_i v_{i,ref} + (\boldsymbol{B}_i - \boldsymbol{E}_i) i_{i,ref} + \frac{\boldsymbol{C}}{N} \right] \right\} \tag{15}$$

where $\mathbb{V}=\{v_{i,ref}|\underline{v}\le v_{i,ref}\le\bar{v}\}$ and $\mathbb{I}=\{i_{i,ref}|\underline{i}_i\le i_{i,ref}\le\bar{i}_i\}$ are the feasible regions of $\boldsymbol{V}_{ref}$ and $\boldsymbol{I}_{ref}$ to fulfill constraints (9) and (10), respectively; $\boldsymbol{\lambda}^i$ is the local estimation of dual vector related to constraint (14), and $\boldsymbol{\lambda}=[\boldsymbol{\lambda}^1,\boldsymbol{\lambda}^2,\ldots,\boldsymbol{\lambda}^N]^{\mathrm{T}}$ is the matrix consist of estimations in each controller; and $\boldsymbol{A}_i$, $\boldsymbol{B}_i$, and $\boldsymbol{E}_i$ are the i^{th} columns of $\boldsymbol{A}$, $\boldsymbol{B}$, and $\boldsymbol{E}$, respectively. As Salter's condition (Assumption 2) holds, strong duality is achieved [34]. Therefore, the optimization problem in (6) is equivalent to (16).

$$\begin{cases}\max\ \phi(\boldsymbol{\lambda})\\ \text{s.t. } \boldsymbol{\lambda}^i=\boldsymbol{\lambda}^j\\ \quad\forall i,j=\{1,2,...,N\}\end{cases}\tag{16}$$

In addition, $v_{i,ref}$ and $i_{i,ref}$ can be solved analytically as:

$$\begin{cases}v_{i,ref}=\left[v_{nom}-\dfrac{(\boldsymbol{\lambda}^i)^{\mathrm{T}}\boldsymbol{A}_i}{2\beta}\right]_{\underline{v}}^{\bar{v}}\\ i_{i,ref}=\left[-\dfrac{2\alpha b_i+(\boldsymbol{\lambda}^i)^{\mathrm{T}}(\boldsymbol{B}_i-\boldsymbol{E}_i)}{2\alpha a_i}\right]_{\underline{i}_i}^{\bar{i}_i}\end{cases}\tag{17}$$

where the projection function $[x]_a^b=\max(a,\min(x,b))$ is defined to limit $v_{i,ref}$ and $i_{i,ref}$ within the feasible region.

Based on Lemma 1 presented in [34], the gradient of $\phi(\boldsymbol{\lambda})$ is defined as:

$$\nabla\phi(\boldsymbol{\lambda})=\boldsymbol{A}\boldsymbol{V}_m+(\boldsymbol{B}-\boldsymbol{E})\boldsymbol{I}_m+\frac{1}{N}\boldsymbol{C}\boldsymbol{1}^{\mathrm{T}}\tag{18}$$

where $\boldsymbol{V}_m=\mathrm{diag}\{v_{1,ref},v_{2,ref},\ldots,v_{N,ref}\}$ and $\boldsymbol{I}_m=\mathrm{diag}\{i_{1,ref},i_{2,ref},\ldots,i_{N,ref}\}$. It is impossible to calculate the gradient $\nabla\phi(\boldsymbol{\lambda})$ without communication as it requires the information of the entire system. However, the current imbalance $\boldsymbol{g}(\boldsymbol{\lambda})=\boldsymbol{I}-\boldsymbol{I}_{ref}$ can be directly measured by each converter, which provides the information gradient $\nabla\phi(\boldsymbol{\lambda})$. Combining (12) and (16) yields:

$$g_i(\boldsymbol{\lambda})=i_i-i_{i,ref}=\sum_{j=1}^{N}\frac{\partial\phi(\boldsymbol{\lambda})}{\partial\lambda_i^j}\tag{19}$$

where $g_i(\boldsymbol{\lambda})$ and λ_i^j are the i^{th} elements of $\boldsymbol{g}(\boldsymbol{\lambda})$ and $\boldsymbol{\lambda}^j$, respectively.

The pseudocode of the OPF algorithm is shown in Algorithm 1. In the algorithm, we define $\boldsymbol{y}^i$ as the local estimation of $\boldsymbol{g}$ for controller i; $\boldsymbol{y}=[\boldsymbol{y}^1,\boldsymbol{y}^2,\ldots,\boldsymbol{y}^n]^{\mathrm{T}}$ is the status matrix of the entire system. In addition, y_j^i is the j^{th} element of vector $\boldsymbol{y}^i$; $\boldsymbol{s}^i$ and $\boldsymbol{q}^i$ are the temporary variable vectors exchanged between converters; and γ is the step size of the system.

In the initial stage, the initial values of the local variables $\boldsymbol{\lambda}^i$, $v_{i,ref}$, and $i_{i,ref}$ are constants. The current imbalance $i_i-i_{i,ref}$ can be measured using a local controller, which is used to set $\boldsymbol{y}^i$. In this paper, the iteration k is only used to distinguish the current and next iterations. In real-time operations, this variable is not recorded. The controller only requires the current status of the local variables, and the historical variables would not be recorded. Any DG connected to the microgrid initializes its local variables based on constants and local measurements. It can then be introduced into the algorithm. This implies that the plug-and-play capacity is not affected by the initialization stage of the proposed algorithm.

Algorithm 1: secondary control level of OPF algorithm

Step 1: initialization. For each converter, set the iteration $k=0$, $\boldsymbol{\lambda}^i(0)=\boldsymbol{0}$; initialize $v_{i,ref}(0)=v_{nom}$ and $i_{i,ref}(0)=-b_i/(2a_i)$; measure the local current imbalance $g_i(\boldsymbol{\lambda}(0))=i_i(0)-i_{i,ref}(0)$; and set $y_i^i(0)=Ng_i(\boldsymbol{\lambda}(0))$, while other elements of $\boldsymbol{y}^i$ are initialized to be 0.

Step 2: local optimization of $\boldsymbol{\lambda}^i$. For controller i, compute:

$$\begin{cases}\boldsymbol{s}^i(k)=\boldsymbol{\lambda}^i(k)-\gamma\boldsymbol{y}^i(k)\\ \boldsymbol{\lambda}^i(k+1)=\boldsymbol{s}^i(k)+\sum\limits_{j\in N_i}w_{ij}(k)(\boldsymbol{s}^i(k)-\boldsymbol{s}^i(k))\end{cases}$$

Step 3: primary problem solution. Calculate primary variables $v_{i,ref}(k+1)$ and $i_{i,ref}(k+1)$ by:

$$\begin{cases}v_{i,ref}(k+1)=\left[v_{nom}-\dfrac{(\boldsymbol{\lambda}^i(k))^{\mathrm{T}}\boldsymbol{A}_i}{2\beta}\right]_{\underline{v}}^{\bar{v}}\\ i_{i,ref}(k+1)=\left[-\dfrac{b_i+(\boldsymbol{\lambda}^i(k))^{\mathrm{T}}(\boldsymbol{B}_i-\boldsymbol{E}_i)}{2\alpha a_i}\right]_{\underline{i}_i}^{\bar{i}_i}\end{cases}$$

Step 4: dynamic average consensus of $\boldsymbol{y}^i$. Measure the current imbalance $g_i(\boldsymbol{\lambda}(k+1))=i_i(k+1)-i_{i,ref}(k+1)$ under new references $v_{i,ref}(k+1)$ and $i_{i,ref}(k+1)$. Then, update $\boldsymbol{y}^i(k+1)$ with

$$\begin{cases}q_i^i(k)=y_i^i(k)+N\left(g_i(\boldsymbol{\lambda}(k+1))-g_i(\boldsymbol{\lambda}(k))\right)\\ q_j^i(k)=y_j^i(k)\qquad\forall j\ne i\\ \boldsymbol{y}^i(k+1)=\boldsymbol{q}^i(k)+\sum\limits_{j\in N_i}w_{ij}(k)(\boldsymbol{q}^i(k)-\boldsymbol{q}^i(k))\end{cases}$$

Step 5: set k: $k+1$ and go to *Step 2*.

Remark 2: in the proposed algorithm, only the generator cost is considered. If other power management algorithms exist such as energy storage management algorithms, the controlled devices are considered non-dispatchable ones. This means that the proposed algorithm can work in parallel with other real-time power management algorithms.

Remark 3: in the proposed algorithm, a quadratic cost function is applied. If another convex function is applied as a cost function, *Step 3* would become an optimal problem to solve $v_{i,ref}$ and $i_{i,ref}$ based on local variables. This problem can be solved using a local controller. However, a non-convex cost function cannot be applied because it makes the OPF problem non-convex.

The convergence and optimality of the proposed algorithm are then given in Theorem 1.

Theorem 1: assuming that Assumptions 1 and 2 hold, consider the sequences $\boldsymbol{\lambda}(k)$ and $\boldsymbol{y}(k)$ generated by the proposed algorithm. Let the vector $\bar{\boldsymbol{\lambda}}(k)=\boldsymbol{J}\boldsymbol{\lambda}(k)$ be an average matrix and $\tilde{\boldsymbol{\lambda}}(k)=\boldsymbol{\lambda}(k)-\bar{\boldsymbol{\lambda}}(k)$ is the corresponding disagreement matrix. Then, a positive number γ^* exists such that if $\gamma\le\gamma^*$, we have $\lim\limits_{k\to\infty}\tilde{\boldsymbol{\lambda}}(k)=\boldsymbol{0}$ and $\lim\limits_{k\to\infty}\phi(\boldsymbol{\lambda}(k))=\phi^*$, where ϕ^* is the solution to (16).

The proof of Theorem 1 is inspired by [35]. In [35], an unconstrained distributed optimization method is provided for stochastic communication networks. Thus, the original OPF problem is converted to a dual problem, which aims to solve the dual variable $\boldsymbol{\lambda}$. A major obstacle is that $\phi(\boldsymbol{\lambda})$ is coupled between different agents, which differs from the assumption in [35]. To solve this problem, we use $g(\boldsymbol{\lambda})$, which can be directly measured by each agent, to obtain the information about $\nabla\phi(\boldsymbol{\lambda})$.

The detailed proof is given in Appendix A.

IV. Case Study

A. Test System

To validate the effectiveness of the proposed algorithm, a DC microgrid utilizing the skeleton of the IEEE 30-bus test feeder system is set, as shown in Fig. 2. We choose IEEE 30-bus test system as the skeleton because it is a meshed grid that can verify our algorithm in a microgrid with meshed structure. The nominal voltage of the DC microgrid is set to be 1000 V within the ±5% deviation range. The line resistance values are listed in Table I.

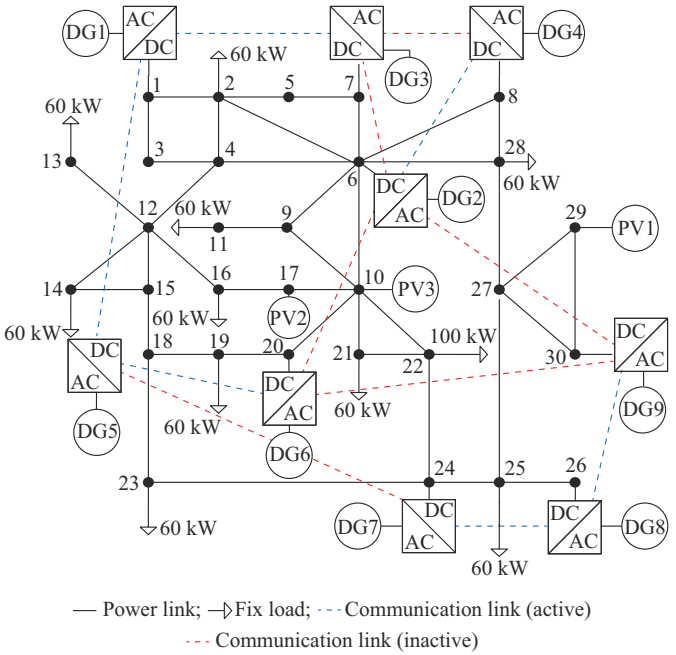

Fig. 2. Test system for proposed algorithm.

TABLE I
Line Resistance Values

Line No.	Resistance (Ω)	Line No.	Resistance (Ω)	Line No.	Resistance (Ω)
1-2	0.06	1-3	0.19	2-4	0.17
3-4	0.04	2-5	0.02	2-6	0.18
4-6	0.04	5-7	0.12	6-7	0.08
6-8	0.04	6-9	0.21	6-10	0.56
9-11	0.21	9-10	0.11	4-12	0.26
12-13	0.14	12-14	0.26	12-15	0.13
12-16	0.20	14-15	0.20	16-17	0.19
15-18	0.22	18-19	0.13	19-20	0.07
10-20	0.21	10-17	0.08	10-21	0.07
10-22	0.15	21-22	0.02	15-23	0.20
22-24	0.18	23-24	0.27	24-25	0.33
25-26	0.38	25-27	0.21	28-27	0.40
27-29	0.42	27-30	0.60	29-30	0.45
8-28	0.20	6-28	0.06		

The interval time of the secondary control is set to be 0.2 s. In this paper, each communication link is assumed to be subject to random failure following a certain Bernoulli process. In other words, in each iteration, each communication link will be activated with a probability of p or deactivated with a probability of $1-p$. Thus, when $p=1$, the simulation is retrograded to a fixed scenario. In this paper, p is set to be 0.5 in most scenarios except for a special statement.

Nine DGs are modeled as Capstone microturbines, which are connected to DC mircrogird via power electronic converters. The proposed controller is also integrated in converters. The economic parameters of DGs are shown in Table II. Three PV plants are set to generate 100 kW power. We set the droop coefficient $m=1$ and the step size $\gamma=0.03$. The trade-off parameters are set as $\alpha=1$ and $\beta=0.01$.

TABLE II
Economic Parameters of DGs

Model	DG No.	Economic parameter			I_{max} (A)	I_{min} (A)
		a_i (¢/kW^{2}h)	b_i (¢/kWh)	c_i (¢/h)		
Capstone 330 (high pressure)	DG1	0.0248	2.366	21.43	28	5
Capstone 330 (liquid fuel)	DG2, DG5	0.0680	1.730	21.46	26	5
Capstone C65	DG3, DG7, DG8	0.0045	3.253	29.51	65	5
Capstone C200	DG4, DG6, DG9	0.0019	2.232	82.33	200	5

B. Accuracy Validation

To validate the accuracy of the proposed algorithm, the CVX tool [36] in MATLAB is used to solve the original problem given in (5). As shown in Table III, the optimal solutions of problem (5) solved by CVX, the steady-state bus voltages and output currents controlled by proposed algorithm, and the relative errors between the optimal solutions and the steady-state values are listed. It can be derived that relative error is less than 0.6%, which validates the accuracy of the proposed algorithm.

TABLE III
Accuracy Comparison

DG No.	CVX		Proposed algorithm		Relative error (%)	
	Voltage (V)	Current (A)	Voltage (V)	Current (A)	Voltage	Current
DG1	992.1	9.96	992.1	9.99	0	0.305
DG2	995.9	8.18	995.9	8.19	0	0.065
DG3	995.3	5.00	995.3	5.00	0	0.000
DG4	1001.3	159.54	1001.3	159.52	0	–0.016
DG5	989.4	8.52	989.4	8.51	0	0.077
DG6	1003.7	166.62	1003.7	166.62	0	–0.002
DG7	983.4	5.00	983.4	5.03	0	0.577
DG8	996.6	5.00	996.6	5.00	0	0.090
DG9	1042.1	32.16	1042.1	32.17	0	0.041

C. Dynamic Process

As in a time-varying environment, the available power of PVs fluctuates rapidly over time [37]-[39]. In this subsection, the impact of the load change and PV fluctuation are

analyzed. In this scenario, the power of PV1 drops by 80% of the output power at a speed of 8 kW/s at $t=10$ s. The power of PV1 recovers at the same speed at $t=60$ s. These fluctuations resemble those reported in [37]-[39]. In addition, a new load $L=70$ kW connected to bus 3 begins to drain the power at $t=40$ s. Dynamic output currents of DG1-DG4 and dynamic bus voltages of DG7 and DG9 are shown in Fig. 3.

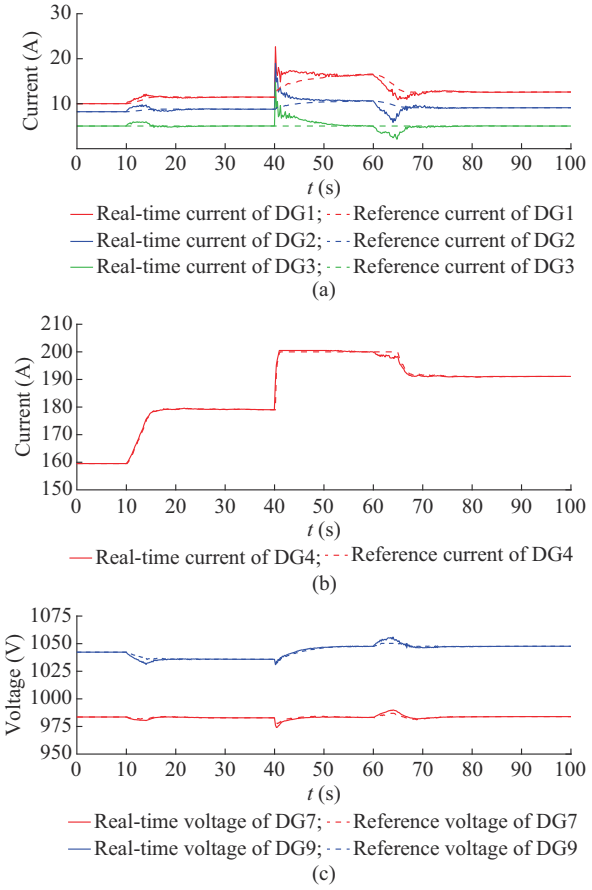

Fig. 3. Dynamic output currents of DG1-DG4 and dynamic bus voltages of DG7 and DG9. (a) Dynamic output currents of DG1-DG3. (b) Dynamic output current of DG4. (c) Bus voltages of DG7 and DG9.

DG1-DG4 are four different types of generators for the output current; DG7 and DG9 have the maximum and minimum bus voltages, respectively. After the PV power drops, all DGs begin to increase the output power to maintain the power balance. Simultaneously, the secondary control also adjusts references $i_{i,ref}$ and $v_{i,ref}$ to find the new optimal working point of the system. Finally, both the current injection and bus voltage converge to the optimal solution shortly after the PV power stops decreasing. Similarly, when the PV power recovers, the DGs decrease their power outputs to reach the new optimum. After the loads are connected to the microgrid, the output current i_i of each converter immediately increases to satisfy the power balance derived from the primary control. The secondary control then begins to adjust the references $i_{i,ref}$ and $v_{i,ref}$ to find the new optimal working point of the microgrid. Finally, both the current injection and bus voltage converge to an optimal solution within 20 s. It can also be observed that the ranges of the current and voltage are recovered after the transient process. In summary, the proposed algorithm can drive the microgrid to a new optimal state under fluctuating PV and load power.

D. System Performance Under Different Communication Failure Ratios

Next, the dynamic current injection of DG1 using the proposed algorithm under different p is examined in Fig. 4.

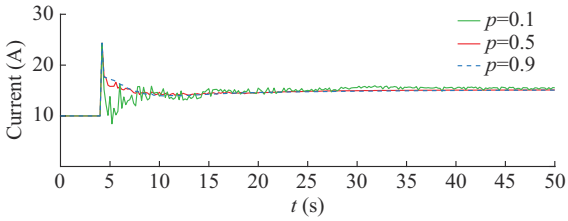

Fig. 4. Dynamic current injection of DG1 under different p.

In this scenario, a new load $L=70$ kW connected to bus 3 starts to drain the power at $t=4$ s. Simultaneously, the power of PV4 drops to 70 kW. When p is close to 1, e.g., $p=0.9$, the curve is smooth and resembles the dynamics of the fixed topology case. When p is low, e.g., $p=0.1$, which means that only 10% of communication is successful, the oscillation occurs and the convergence is slower. However, the algorithm still converges to the optimal solution. The ability of the proposed algorithm to withstand communication failure is thus validated. To investigate the effect of p on the convergence time, a Monte Carlo test is performed. The simulation contains 10 sets with even distributed p from 0.1 to 1. Each set contains 500 cases. A box plot of Monte Carlo test of convergence time is presented in Fig. 5, where the middle-horizon red line represents the median of each set, the blue box represents the middle 50% of all cases, and the vertical blue lines represent the ranges of all cases.

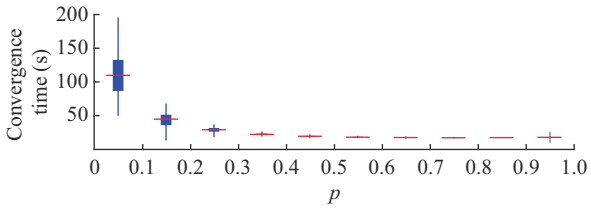

Fig. 5. Box plot of Monte Carlo test of convergence time with different p.

If $p=0.1$, the convergence is slow. The median of the convergence time is approximately 110 s. In addition, the convergence time is distributed in a long range from 50 s to 200 s, which means that the randomness has a tremendous effect on the convergence. When p increases, the convergence becomes faster and the distribution range becomes narrower. This indicates that with a larger p, the randomness will have a smaller effect on the convergence. When $p\geq 0.5$, the convergence time stops decreasing and nearly all cases converge at the same time. It could be observed that under these cases, the random communication failures have little effect on the convergence and the system behavior is similar

to one without random communication failure.

E. System Performance Under Communication Delay

To verify the performance of the proposed algorithm under a communication delay, the dynamic response of the proposed algorithm under random communication is performed. The delay time is set randomly between 0 s and 2 s, and the failure ratio of the communication remains 50%. The dynamic current injection of DG1 under a random communication delay of 0-2 s is illustrated in Fig. 6. It could be concluded that the algorithm converges to an optimal solution under a random delay. However, the oscillation occurs and the algorithm converges more slowly. Again, it could be concluded that the algorithm could operate under a communication delay. However, this delay will degrade the performance of the algorithm.

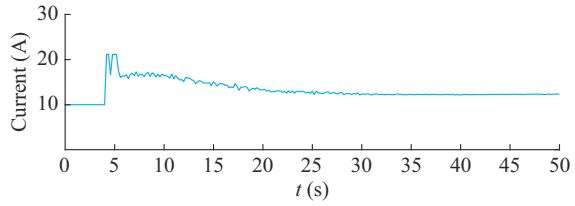

Fig. 6. Dynamic current injection of DG1 under a random communication delay of 0-2 s.

F. Plug-and-play Capacity

The plug-and-play capacity of the proposed algorithm is illustrated in Fig. 7.

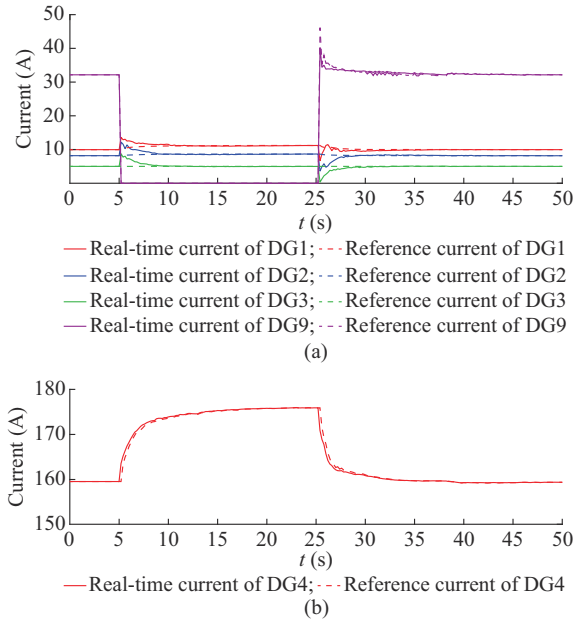

Fig. 7. Plug-and-play capacity of proposed algorithm. (a) Dynamic output currents of DG1-DG3 and DG9. (b) Dynamic output current of DG4.

The dynamic responses of DG1-DG4 and DG9 are provided. When DG9 is disconnected from the microgrid at $t=5$ s, other DGs increase their outputs to compensate the power imbalance derived from the disconnection. The secondary control then navigates the microgrid to a new optimal point in 10 s. At $t=25$ s, DG9 is recovered. The outputs of other DGs decrease. The secondary control starts to lower the reference current to recover the original optimal point. Finally, the system returns to its original working point at $t=45$ s.

G. Comparison of Original and Simplified Models

Finally, to justify the rationality of the simplification of the OPF problem as described in Section II, a Monte Carlo test containing 4000 cases is performed to compare the solutions of the OPF problems (3)-(5). In each case, the parameters of the system are selected with a normal distribution with expectation μ and variance σ. The system setup for Monte Carlo simulation is presented in Table IV.

TABLE IV
SYSTEM SETUP FOR MONTE CARLO SIMULATION

Parameter	μ	σ	Parameter	μ	σ
a_i	0.03	0.01	$I_{\max}$ (A)	100	33
b_i	3.00	1.00	$I_{\min}$ (A)	5	1
c_i	50.00	25.00	Load (kW)	100	33

First, all random cases are solved based on the simplified model (5) to obtain a sub-optimal solution. Then, the global optimization method provided by MATLAB, which uses the scatter-search mechanism, is used to find the optimal solution of (5). The relative error E_r between the two models is calculated by:

$$E_r = \frac{J_{sub} - J_{opt}}{J_{opt}} \tag{20}$$

where J_{opt} and J_{sub} are the values of the objective function based on the original model (3) and simplified model (5), respectively.

A histogram of relative error E_r is shown in Fig. 8. It could be concluded that the relative error is less than 1% for all cases. In addition, in most cases, the relative error is less than 0.3%. Based on the aforementioned discussion, we could conclude that the simplification described in Section II is reasonable.

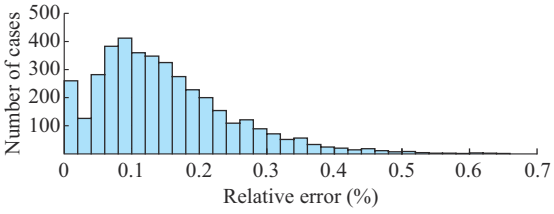

Fig. 8. Histogram of relative error.

V. CONCLUSION AND FUTURE WORK

In this paper, a real-time OPF algorithm for DC microgrids is proposed. We prove that our algorithm converges to the optimal solution, even under a stochastic communication network. This aspect significantly enhances the reliability of the proposed algorithm. Moreover, our algorithm can obtain information from non-dispatchable devices by local measurement of dispatchable devices, which significantly re-

duces the need for controllers and communication lines. To validate our algorithm, simulations on a IEEE 30-bus DC microrid are adopted including the accuracy, dynamic performance, and plug-and-play capacity.

Our future research will attempt to extend the algorithm to the following scenarios.

1) The proposed algorithm will be extended for OPF control for AC microgrids.

2) Because the proposed algorithm is not suitable for microgrids with varying electrical topologies, developing an algorithm that can solve the OPF problem under these conditions is an interesting topic for future work. The proposed algorithm is validated under random communication delay, but analytical analysis of the performance of the proposed algorithm under communication delay remains an open problem.

APPENDIX A

A. Preliminary

In our proof, we use $\|\boldsymbol{X}\|_F$, $\|\boldsymbol{X}\|_1$, and $\|\boldsymbol{X}\|_2$ for the Frobenius norm, 1-norm, and 2-norm of matrix $\boldsymbol{X}$, respectively, and $\langle \boldsymbol{A}, \boldsymbol{B} \rangle_F$ for the Frobenius inner product of two matrices. We define the average vector $\overline{\boldsymbol{X}} = \boldsymbol{J}\boldsymbol{X}$, where all its elements are equal to the average of the elements of vector $\boldsymbol{X}$. Several important lemmas are presented before the optimum and convergence of the proposed algorithm are discussed.

Lemma 1: an equation is given as $\langle \boldsymbol{A}, \overline{\boldsymbol{B}} \rangle_F = \langle \overline{\boldsymbol{A}}, \boldsymbol{B} \rangle_F$.

Proof 1: based on the definition of the Frobenius inner product, we have:

$$\langle \boldsymbol{A}, \overline{\boldsymbol{B}} \rangle_F = \mathrm{tr}(\boldsymbol{A}^{\mathrm{T}} \boldsymbol{J}\boldsymbol{B}) = \mathrm{tr}((\boldsymbol{J}\boldsymbol{A})^{\mathrm{T}} (\boldsymbol{J}\boldsymbol{B})) = \langle \overline{\boldsymbol{A}}, \overline{\boldsymbol{B}} \rangle_F \tag{A1}$$

where the third equality is derived from $\boldsymbol{J} = \boldsymbol{J}^2$.

Lemma 2: let $\tilde{\boldsymbol{\lambda}}(k) = \boldsymbol{\lambda}(k) - \overline{\boldsymbol{\lambda}}(k)$ and $\tilde{\boldsymbol{y}}(k) = \boldsymbol{y}(k) - \overline{\boldsymbol{y}}(k)$ be the corresponding disagreement matrices. Let $X(k) = \sqrt{E\left(\sum_{i=0}^{k} \|\tilde{\boldsymbol{\lambda}}(k)\|^2\right)}$, $Y(k) = \sqrt{E\left(\sum_{i=0}^{k} \|\tilde{\boldsymbol{y}}(k)\|^2\right)}$, and $Z(k) = \sqrt{E\left(\sum_{i=0}^{k} \|\overline{\boldsymbol{y}}(k)\|^2\right)}$ be expected energy from 0 to k. Then, we have:

$$X(k) \le \frac{s_1 p_2}{1 - s_1 s_2} Z(k) + \frac{q_1 + s_1 q_2}{1 - s_1 s_2} \tag{A2}$$

$$Y(k) \le \frac{p_2}{1 - s_1 s_2} kZ(k) + \frac{q_2 + s_1 q_1}{1 - s_1 s_2} \tag{A3}$$

where $s_1 = \dfrac{\sqrt{2}\,\gamma\eta}{1-\eta}$; $q_1 = \dfrac{\sqrt{2}\,E\left(\|\tilde{\boldsymbol{\lambda}}(0)\|_2\right)}{\sqrt{1-\eta^2}}$; $s_2 = \dfrac{\sqrt{2}\,NL(1+\eta)}{1-\eta}$; $p_2 = \dfrac{\sqrt{2}\,NL(1+\eta)\gamma}{1-\eta}$; and $q_2 = \dfrac{\sqrt{2}\,E\left(\|\tilde{\boldsymbol{y}}(0)\|_2\right)}{\sqrt{1-\eta^2}}$.

Proof 2: since $\boldsymbol{W}_k \boldsymbol{J} = \boldsymbol{J}\boldsymbol{W}_k = \boldsymbol{J}$, we could obtain:

$$\tilde{\boldsymbol{\lambda}}(k+1) = \boldsymbol{A}_k (\tilde{\boldsymbol{\lambda}}(k) - \gamma \tilde{\boldsymbol{y}}(k)) \tag{A4}$$

where $\boldsymbol{A}_k = \boldsymbol{W}_k - \boldsymbol{J}$. Then, based on the inequality of the 2-norm [40], we have:

$$E\left(\|\tilde{\boldsymbol{\lambda}}(k+1)\|_2\right) = E\left(\|\boldsymbol{A}_k(\tilde{\boldsymbol{\lambda}}(k) - \gamma\tilde{\boldsymbol{y}}(k))\|_2\right) \le E\left(\|\boldsymbol{A}_k \tilde{\boldsymbol{\lambda}}(k)\|_2\right) + E\left(\|\gamma \boldsymbol{A}_k \tilde{\boldsymbol{y}}(k)\|_2\right) \le \eta E\left(\|\tilde{\boldsymbol{\lambda}}(k)\|_2\right) + \gamma\eta E\left(\|\tilde{\boldsymbol{y}}(k)\|_2\right) \tag{A5}$$

According to the convergence property of energy of random variables [35], let $v(k) = E\left(\|\tilde{\boldsymbol{\lambda}}(k)\|_2\right)$ and $w(k) = \gamma\eta E\left(\|\tilde{\boldsymbol{y}}(k)\|_2\right)$, and then we have:

$$X(k) \le s_1 Y(k) + q_1 \tag{A6}$$

Similarly, we can yield:

$$\tilde{\boldsymbol{y}}(k+1) = \boldsymbol{A}_k \tilde{\boldsymbol{y}}(k) + \boldsymbol{A}_k \Delta \boldsymbol{g}_m(\boldsymbol{\lambda}(k))) \tag{A7}$$

Then, taking the norm expectation of both sides yields:

$$\begin{aligned} &E\left(\|\tilde{\boldsymbol{y}}(k+1)\|_2\right) \le E\left(\|\boldsymbol{A}_k \tilde{\boldsymbol{y}}(k)\|_2\right) + E\left(\|\boldsymbol{A}_k \Delta \boldsymbol{g}_m(\boldsymbol{\lambda}(k))\|_2\right) \overset{①}{\le} \\ &\eta E\left(\|\tilde{\boldsymbol{y}}(k)\|_2\right) + E\left(|\max\left(\boldsymbol{g}(\boldsymbol{\lambda}(k+1)) - \boldsymbol{g}(\boldsymbol{\lambda}(k))\right)|\right) \overset{②}{\le} \\ &\eta E\left(\|\tilde{\boldsymbol{y}}(k)\|_2\right) + E\left(\|\nabla\phi(\boldsymbol{\lambda}(k+1)) - \nabla\phi(\boldsymbol{\lambda}(k))\|_1\right) \overset{③}{\le} \\ &\eta E\left(\|\tilde{\boldsymbol{y}}(k)\|_2\right) + \sqrt{N}\, E\left(\|\nabla\phi(\boldsymbol{\lambda}(k+1)) - \nabla\phi(\boldsymbol{\lambda}(k))\|_F\right) \overset{④}{\le} \\ &\eta E\left(\|\tilde{\boldsymbol{y}}(k)\|_2\right) + \sqrt{N}\, LE\left(\|\tilde{\boldsymbol{\lambda}}(k+1) - \tilde{\boldsymbol{\lambda}}(k) - \gamma\overline{\boldsymbol{y}}(k)\|_F\right) \overset{⑤}{\le} \\ &\eta E\left(\|\tilde{\boldsymbol{y}}(k)\|_2\right) + NL\left(E\left(\|\tilde{\boldsymbol{\lambda}}(k+1)\|_2\right) + E\left(\|\tilde{\boldsymbol{\lambda}}(k)\|_2\right) + \gamma E\left(\|\overline{\boldsymbol{y}}(k)\|_2\right)\right) \end{aligned} \tag{A8}$$

where $\Delta \boldsymbol{g}_m(\boldsymbol{\lambda}(k)) = N \cdot \mathrm{diag}\{\boldsymbol{g}(\boldsymbol{\lambda}(k+1)) - \boldsymbol{g}(\boldsymbol{\lambda}(k))\}$; ① is derived from the definition of $\Delta \boldsymbol{g}_m(\boldsymbol{\lambda}(k))$ and the fact that $E\left(\|\boldsymbol{A}_k\|_2\right) < 1$; ② is derived in the next subsection; and ③-⑤ are derived from the inequality between matrix norms [40]. Combining (A5) and (A8) yields:

$$E\left(\|\tilde{\boldsymbol{y}}(k+1)\|_2\right) \le \eta E\left(\|\tilde{\boldsymbol{y}}(k)\|_2\right) + NL(1+\eta)\left(E\left(\|\tilde{\boldsymbol{y}}(k)\|_2\right) + \gamma E\left(\|\tilde{\boldsymbol{y}}(k)\|_2\right)\right) \tag{A9}$$

Utilizing the convergence of the energy of random variables [35] and letting $v(k) = E\left(\|\tilde{\boldsymbol{y}}(k)\|_2\right)$ and $w(k) = NL(1+\eta)\left(E\left(\|\tilde{\boldsymbol{\lambda}}(k)\|_2 + \gamma\|\tilde{\boldsymbol{y}}(k)\|_2\right)\right)$, we obtain:

$$Y(k) \le s_2 X(k) + p_2 Z(k) + q_2 \tag{A10}$$

Combining (A6) and (A10) completes the proof.

Lemma 3: convergence of random sequence. Let $(\Omega, \mathcal{F})$ be a probability space and $\mathcal{F}_0 \subset \mathcal{F}_1 \subset \ldots \subset \mathcal{F}_k$ be a sequence of σ subfields of $\mathcal{F}$. Let $v(k)$, $a(k)$, and $w(k)$ be non-negative random variables, the following relationship then holds for $\forall k \ge 0$:

$$E\left(v(k+1)\,|\,\mathcal{F}\right) \le (1 + a(k))v(k) - u(k) + w(k) \tag{A11}$$

where $\sum_{k=0}^{\infty} a(k) \le \infty$ and $\sum_{k=0}^{\infty} w(k) \le \infty$. Then, $v(k)$ converges to some random variables v, and we further have $\sum_{k=0}^{\infty} u(k) \le \infty$.

B. Proof of Convergence Theorem

Proof 3: by properly intertwining the optimization and dynamic consensus steps, we can rewrite the proposed algorithm in a compact form as:

$$\boldsymbol{\lambda}(k+1) = \boldsymbol{W}_k(\boldsymbol{\lambda}(k) - \gamma \boldsymbol{y}(k)) \tag{A12}$$

$$\boldsymbol{y}(k+1) = \boldsymbol{W}_k(\boldsymbol{y}(k) + \Delta \boldsymbol{g}_m(\boldsymbol{\lambda}(k))) \tag{A13}$$

To investigate the convergence properties of the proposed algorithm, we first consider the following auxiliary sequence

that runs analogously to (A12) and (A13) in the average space:

$$\bar{\boldsymbol{\lambda}}(k+1)=\bar{\boldsymbol{\lambda}}(k)-\gamma\bar{\boldsymbol{y}}(k) \tag{A14}$$

$$\bar{\boldsymbol{y}}(k+1)=\bar{\boldsymbol{y}}(k)+\Delta\bar{\boldsymbol{g}}_m(\boldsymbol{\lambda}(k)) \tag{A15}$$

Function $\phi(\boldsymbol{\lambda})$ is a concave second-order Lipschitz continuity with constant L. In other words, for $\forall\boldsymbol{\lambda}_1,\boldsymbol{\lambda}_2\in\mathcal{R}^{n\times n}$, we have:

$$\phi(\boldsymbol{\lambda}_2)\le\phi(\boldsymbol{\lambda}_1)+\left\langle\nabla\phi(\boldsymbol{\lambda}_1),\boldsymbol{\lambda}_2-\boldsymbol{\lambda}_1\right\rangle_F+\frac{L}{2}\|\boldsymbol{\lambda}_2-\boldsymbol{\lambda}_1\|_F^2 \tag{A16}$$

In addition, based on (A16) and the conservation property of the averaging matrix [42], we immediately obtain:

$$\nabla\bar{\boldsymbol{\phi}}(\boldsymbol{\lambda}(k))=\boldsymbol{J}\nabla\phi(\boldsymbol{\lambda}(k))=\bar{\boldsymbol{g}}_m(\boldsymbol{\lambda}(k))=\bar{\boldsymbol{y}}(k) \tag{A17}$$

Taking conditional expectation on $\mathcal{F}_k$ and plugging $\boldsymbol{\lambda}_2=\bar{\boldsymbol{\lambda}}(k+1)$ and $\boldsymbol{\lambda}_1=\bar{\boldsymbol{\lambda}}(k)$ into (A16) yields:

$$\begin{aligned}E(\phi(\bar{\boldsymbol{\lambda}}(k+1)))&\overset{①}{\le}\phi(\bar{\boldsymbol{\lambda}}(k))-\gamma\left\langle\nabla\phi(\bar{\boldsymbol{\lambda}}(k)),\bar{\boldsymbol{y}}(k)\right\rangle_F+\\&\frac{L\gamma^2}{2}\|\bar{\boldsymbol{y}}(k)\|_F^2\overset{②}{=}\phi(\bar{\boldsymbol{\lambda}}(k))-\gamma\left\langle\nabla\bar{\boldsymbol{\phi}}(\boldsymbol{\lambda}(k),\bar{\boldsymbol{y}}(k)\right\rangle_F+\\&\frac{L\gamma^2}{2}\|\bar{\boldsymbol{y}}(k)\|_F^2+\gamma\left\langle\nabla\bar{\boldsymbol{\phi}}(\boldsymbol{\lambda}(k)-\nabla\phi(\bar{\boldsymbol{\lambda}}(k))),\bar{\boldsymbol{y}}(k)\right\rangle_F\overset{③}{=}\phi(\bar{\boldsymbol{\lambda}}(k))-\\&\gamma\|\bar{\boldsymbol{y}}(k)\|_F^2+\frac{L\gamma^2}{2}\|\bar{\boldsymbol{y}}(k)\|_F^2+\gamma\left\langle\nabla\bar{\boldsymbol{\phi}}(\boldsymbol{\lambda}(k)-\nabla\phi(\bar{\boldsymbol{\lambda}}(k))),\bar{\boldsymbol{y}}(k)\right\rangle_F\end{aligned} \tag{A18}$$

where ① and ③ are derived from (A16) and (A17), respectively. In addition, based on the Lipschitz continuity of $\phi(\boldsymbol{\lambda})$, we have:

$$\begin{aligned}&\left\langle\nabla\bar{\boldsymbol{\phi}}(\boldsymbol{\lambda}(k)-\nabla\phi(\bar{\boldsymbol{\lambda}}(k))),\bar{\boldsymbol{y}}(k)\right\rangle_F=\left\langle\nabla\bar{\boldsymbol{\phi}}(\boldsymbol{\lambda}(k),\bar{\boldsymbol{y}}(k)\right\rangle_F-\\&\left\langle\nabla\phi(\bar{\boldsymbol{\lambda}}(k)),\bar{\boldsymbol{y}}(k)\right\rangle_F=\left\langle\nabla\phi(\boldsymbol{\lambda}(k)),\bar{\boldsymbol{y}}(k)\right\rangle_F-\\&\left\langle\nabla\phi(\bar{\boldsymbol{\lambda}}(k)),\bar{\boldsymbol{y}}(k)\right\rangle_F=\left\langle\nabla\phi(\boldsymbol{\lambda}(k))-\nabla\phi(\bar{\boldsymbol{\lambda}}(k)),\bar{\boldsymbol{y}}(k)\right\rangle_F\le\\&\|\nabla\phi(\boldsymbol{\lambda}(k))-\nabla\phi(\bar{\boldsymbol{\lambda}}(k))\|_F\|\bar{\boldsymbol{y}}(k)\|_F\le L\|\tilde{\boldsymbol{\lambda}}(k)\|_F\|\bar{\boldsymbol{y}}(k)\|_F\end{aligned} \tag{A19}$$

Combining (A18) and (A19) yields:

$$E(\phi(\bar{\boldsymbol{\lambda}}(k+1)))\le\phi(\bar{\boldsymbol{\lambda}}(k))-\left(\gamma-\frac{L\gamma^2}{2}\right)\|\bar{\boldsymbol{y}}(k)\|_F^2+\gamma L\|\tilde{\boldsymbol{\lambda}}(k)\|_F\|\bar{\boldsymbol{y}}(k)\|_F \tag{A20}$$

Let $v(k)=\phi(\bar{\boldsymbol{\lambda}}(k))$ and we have:

$$E(v(k+1))\le v(k)-a'\|\bar{\boldsymbol{y}}(k)\|_2^2+\gamma NL\|\tilde{\boldsymbol{\lambda}}(k)\|_2\|\bar{\boldsymbol{y}}(k)\|_2 \tag{A21}$$

where $a'=N\gamma^2\left(1/\gamma-L/2\right)$.

Taking the total expectation and sum (A21) from 0 to k, we obtain:

$$\begin{aligned}&E(v(k+1))\le E(v(0))-a'E\left(\sum_{i=0}^{k}\|\bar{\boldsymbol{y}}(i)\|_2^2\right)+\\&\gamma NLE\left(\sum_{i=0}^{k}\|\tilde{\boldsymbol{\lambda}}(i)\|_2\|\bar{\boldsymbol{y}}(i)\|_2\right)\le E(v(0))-a'Z^2(k)+\gamma NLX(k)Z(k)\end{aligned} \tag{A22}$$

Then, the last inequality is derived from the Cauchy-Schwarz inequality.

Invoking Lemma 2, we obtain:

$$X(k)Z(k)\le b_1Z^2(k)+b_2Z(k) \tag{A23}$$

where $b_1=\dfrac{s_1p_2}{1-s_1s_2}$ and $b_2=\dfrac{q_1+s_1q_2}{1-s_1s_2}$.

Combining (A21) and (A22) yields:

$$E(v(k+1))\le E(v(0))-a_0Z^2(k)+b_0Z(k) \tag{A24}$$

where $a_0=a'-\gamma NLb_1$ and $b_0=\gamma NLb_2$ are the constants that depend on η and γ. Because $E(v(k))\ge0$, we have:

$$-a_0Z(k)^2+b_0Z(k)+E(v(0))\ge0 \tag{A25}$$

Based on the definition of a_0, we can derive that $a_0>0$ when the step size γ is sufficiently small. Because $b_0>0$ and $E(v(0))>0$, it follows from (A25) that

$$\lim_{k\to\infty}Z(k)<\infty \tag{A26}$$

Thus, applying Markov's inequality [43] to any $\epsilon>0$, we obtain:

$$\sum_{i=0}^{\infty}P(\|\bar{\boldsymbol{y}}(i)\|_2>\epsilon)\le\frac{\sum_{i=0}^{\infty}E\left(\|\bar{\boldsymbol{y}}(i)\|_2\right)}{\epsilon^2}<\infty \tag{A27}$$

By the Borel-Cantelli Lemma in [43] and Proposition 1.2 in [44], we have $\lim_{k\to\infty}\|\bar{\boldsymbol{y}}_k\|_2=0$. From Lemma 2, we can derive:

$$X(k)\le\frac{s_1p_2+p_1}{1-s_1s_2}Z(k)+\frac{q_1+s_1q_2}{1-s_1s_2}<\infty \tag{A28}$$

It shows that $\lim_{k\to\infty}\|\tilde{\boldsymbol{\lambda}}(k)\|_2=0$. Likewise, using Lemma 2, we can deduce that $Y(k)$ is bounded and $\lim_{k\to\infty}\|\tilde{\boldsymbol{y}}(k)\|_2=0$. Then, using $(a+b)^2\le2a^2+2b^2$, we can rewrite (A21) as:

$$E(v(k+1))\le E(v(k))-u(k)+w(k) \tag{A29}$$

where $u(k)=a'\|\bar{\boldsymbol{y}}(k)\|_2^2$ and $w(k)=2NL(\|\tilde{\boldsymbol{\lambda}}(k)\|^2+\|\bar{\boldsymbol{y}}(k)\|_2^2)$. Based on the previous discussion, we have:

$$\sum_{k=0}^{\infty}w(k)\le2NL\left(\lim_{k\to\infty}X^2(k)+\lim_{k\to\infty}Z^2(k)\right)\le\infty \tag{A30}$$

Then, when Lemma 3 is applied, the sequence $v(k)$ converges to some random variables. Because $\phi(\boldsymbol{\lambda})$ is radically unbounded, $\bar{\boldsymbol{\lambda}}(k)$ is also most likely bounded.

Based on the inequality between Frobenius norm and 2-norm, we have $\lim_{k\to\infty}\|\bar{\boldsymbol{y}}_k\|_F=0$, $\lim_{k\to\infty}\|\tilde{\boldsymbol{y}}_k\|_F=0$, and $\lim_{k\to\infty}\|\tilde{\boldsymbol{\lambda}}_k\|_F=0$.

Because $\phi(\boldsymbol{\lambda})$ is concave and second-order Lipschitz continuity with constant L, we obtain:

$$\begin{aligned}&\phi(\boldsymbol{\lambda}^*)-\phi(\bar{\boldsymbol{\lambda}}(k))\le\left\langle\nabla\phi(\bar{\boldsymbol{\lambda}}(k)),\boldsymbol{\lambda}^*-\bar{\boldsymbol{\lambda}}(k)\right\rangle_F=\\&\left\langle\nabla\phi(\boldsymbol{\lambda}(k)),\boldsymbol{\lambda}^*-\bar{\boldsymbol{\lambda}}(k)\right\rangle_F+\\&\left\langle\nabla\phi(\bar{\boldsymbol{\lambda}}(k))-\nabla\phi(\boldsymbol{\lambda}(k)),\boldsymbol{\lambda}^*-\bar{\boldsymbol{\lambda}}(k)\right\rangle_F=\\&\left\langle\Delta\bar{\boldsymbol{g}}_m(k),\boldsymbol{\lambda}^*-\bar{\boldsymbol{\lambda}}(k)\right\rangle_F+\\&\left\langle\nabla\phi(\bar{\boldsymbol{\lambda}}(k))-\nabla\phi(\boldsymbol{\lambda}(k)),\boldsymbol{\lambda}^*-\bar{\boldsymbol{\lambda}}(k)\right\rangle_F\le\|\bar{\boldsymbol{y}}(k)\|_F\|\boldsymbol{\lambda}^*-\bar{\boldsymbol{\lambda}}(k)\|_F+\\&L\|\tilde{\boldsymbol{\lambda}}(k)\|_F\|\boldsymbol{\lambda}^*-\bar{\boldsymbol{\lambda}}(k)\|_F\end{aligned} \tag{A31}$$

where $\boldsymbol{\lambda}^*$ is the optimum of problem (16). Because $\bar{\boldsymbol{\lambda}}(k)$ is bounded, we can derive that $\|\boldsymbol{\lambda}^*-\bar{\boldsymbol{\lambda}}(k)\|_F\le M$, where M is a constant. Thus, from (A31), and recalling the Lipschitz continuity of $\phi(\boldsymbol{\lambda})$, we can claim that

$$\phi(\boldsymbol{\lambda}^*)-\lim_{k\to\infty}\phi(\bar{\boldsymbol{\lambda}}(k))\le M\lim_{k\to\infty}(\|\bar{\boldsymbol{y}}(k)\|_F+L\|\tilde{\boldsymbol{\lambda}}(k)\|_F)=0 \tag{A32}$$

Based on the definition of $\boldsymbol{\lambda}^*$, we can obtain $\phi(\boldsymbol{\lambda}^*)-\phi(\bar{\boldsymbol{\lambda}}(k))\geq 0$. Combining it with (A32) yields:

$$\lim_{k\to\infty}\phi(\bar{\boldsymbol{\lambda}}(k))=\phi(\boldsymbol{\lambda}^*) \tag{A33}$$

Moreover, based on Cauchy's mean value theorem, we have:

$$\phi(\boldsymbol{\lambda}(k))=\phi(\bar{\boldsymbol{\lambda}}(k))+\left\langle\nabla\phi(\boldsymbol{\lambda}(k)+\xi\tilde{\boldsymbol{\lambda}}(k)),\tilde{\boldsymbol{\lambda}}(k)\right\rangle_F \tag{A34}$$

where $0\leq\xi\leq 1$. Because $\|\boldsymbol{\lambda}(k)+\xi\tilde{\boldsymbol{\lambda}}(k)\|_F\leq\|\boldsymbol{\lambda}(k)\|_F+\xi\|\tilde{\boldsymbol{\lambda}}(k)\|_F$ and $\|\nabla\phi(\boldsymbol{\lambda}(k)+\xi\tilde{\boldsymbol{\lambda}}(k))\|_F$ are both bounded, we have:

$$\lim_{k\to\infty}|\phi(\boldsymbol{\lambda}(k))-\phi(\bar{\boldsymbol{\lambda}}(k))|\leq\lim_{k\to\infty}\|\nabla\phi(\boldsymbol{\lambda}(k)+\xi\tilde{\boldsymbol{\lambda}}(k))\|_F\|\tilde{\boldsymbol{\lambda}}(k)\|_F=0 \tag{A35}$$

Combining (A33) and (A35) yields $\lim_{k\to\infty}\phi(\boldsymbol{\lambda}(k))=\phi(\boldsymbol{\lambda}^*)$, which completes the proof.

REFERENCES

[1] T. Dragičević, X. Lu, J. C. Vasquez *et al*., "DC microgrids–Part I: a review of control strategies and stabilization techniques," *IEEE Transactions on Power Electronics*, vol. 31, no. 7, pp. 4876-4891, Jul. 2016.

[2] F. Gao, R. Kang, J. Cao *et al*., "Primary and secondary control in DC microgrids: a review," *Journal of Modern Power Systems and Clean Energy*, vol. 7, no. 2, pp. 227-242, Mar. 2019.

[3] Q. Shafiee, T. Dragičević, J. C. Vasquez *et al*., "Hierarchical control for multiple DC-microgrids clusters," *IEEE Transactions on Energy Conversion*, vol. 29, no. 4, pp. 922-933, Dec. 2014.

[4] A. Maknouninejad, Z. Qu, F. L. Lewis *et al*., "Optimal, nonlinear, and distributed designs of droop controls for DC microgrids," *IEEE Transactions on Smart Grid*, vol. 5, no. 5, pp. 2508-2516, Sept. 2014.

[5] J. M. Guerrero, J. C. Vasquez, J. Matas *et al*., "Hierarchical control of droop-controlled AC and DC microgrids—a general approach toward standardization," *IEEE Transactions on Industrial Electronics*, vol. 58, no. 1, pp. 158-172, Aug. 2011.

[6] M. Baharizadeh, M. S. Golsorkhi, M. Shahparasti *et al*., "A two-layer control scheme based on *p*-droop characteristic for accurate power sharing and voltage regulation in DC microgrids," *IEEE Transactions on Smart Grid*, vol. 12 no. 4, pp. 2776-2787, Jul. 2021.

[7] Z. Li, Z. Cheng, J. Si *et al*., "Distributed event-triggered secondary control for average bus voltage regulation and proportional load sharing of DC microgrid," *Journal of Modern Power Systems and Clean Energy*, vol. 10 no. 2, pp. 678-688, May 2022.

[8] P. Wang, W. Wang, N. Meng *et al*., "Multi-objective energy management system for DC microgrids based on the maximum membership degree principle," *Journal of Modern Power Systems and Clean Energy*, vol. 6, no. 4, pp. 668-678, Jul. 2018.

[9] J. Xiao, P. Wang, and L. Setyawan, "Hierarchical control of hybrid energy storage system in DC microgrids," *IEEE Transactions on Industrial Electronics*, vol. 62, no. 8, pp. 4915-4924, Aug. 2015.

[10] M. Yazdanian and A. Mehrizi-Sani, "Distributed control techniques in microgrids," *IEEE Transactions on Smart Grid*, vol. 5, no. 6, pp. 2901-2909, Nov. 2014.

[11] Z. Zhang and M. -Y. Chow, "Convergence analysis of the incremental cost consensus algorithm under different communication network topologies in a smart grid," *IEEE Transactions on Power Systems*, vol. 27, no. 4, pp. 1761-1768, Nov. 2012.

[12] S. Yang, S. Tan, and J. Xu, "Consensus based approach for economic dispatch problem in a smart grid," *IEEE Transactions on Power Systems*, vol. 28, no. 4, pp. 4416-4426, Nov. 2013.

[13] W. Zhang, Y. Xu, W. Liu *et al*., "Distributed online optimal energy management for smart grids," *IEEE Transactions on Industrial Informatics*, vol. 11, no. 3, pp. 717-727, Jun. 2015.

[14] F. Dörfler, J. W. Simpson-Porco, and F. Bullo, "Breaking the hierarchy: Distributed control and economic optimality in microgrids," *IEEE Transactions on Control of Network Systems*, vol. 3, no. 3, pp. 241-253, Sept. 2016.

[15] G. Chen, J. Ren, and E. N. Feng, "Distributed finite-time economic dispatch of a network of energy resources," *IEEE Transactions on Smart Grid*, vol. 8, no. 2, pp. 822-832, Mar. 2017.

[16] J. Hu, J. Duan, H. Ma *et al*., "Distributed adaptive droop control for optimal power dispatch in DC microgrid," *IEEE Transactions on Industrial Electronics*, vol. 65, no. 1, pp. 778-789, Jan. 2018.

[17] Y. Li, Z. Zhang, T. Dragičević *et al*., "A unified distributed cooperative control of DC microgrids using consensus protocol," *IEEE Transactions on Smart Grid*, vol. 12, no. 3, pp. 1880-1892, May 2021.

[18] Z. Wang, W. Wu, and B. Zhang, "A distributed control method with minimum generation cost for DC microgrids," *IEEE Transactions on Energy Conversion*, vol. 31, no. 4, pp. 1462-1470, Dec. 2016.

[19] Z. Wang, F. Liu, Y. Chen *et al*., "Unified distributed control of standalone DC microgrids," *IEEE Transactions on Smart Grid*, vol. 10, no. 1, pp. 1013-1024, Jan. 2019.

[20] J. Yang, W. Feng, X. Hou *et al*., "A distributed cooperative control algorithm for optimal power flow and voltage regulation in DC power system," *IEEE Transactions on Power Delivery*, vol. 35, no. 2, pp. 892-903, Apr. 2020.

[21] J. Peng, B. Fan, and W. Liu, "Voltage-based distributed optimal control for generation cost minimization and bounded bus voltage regulation in DC microgrids," *IEEE Transactions on Smart Grid*, vol. 12, no. 1, pp. 106-116, Jan. 2020.

[22] J. Peng, B. Fan, Q. Yang *et al*., "Distributed event-triggered control of DC microgrids," *IEEE Systems Journal*, vol. 15, no. 2, pp. 2504-2514, Jun. 2021.

[23] L. Xing, Q. Xu, F. Guo *et al*., "Distributed secondary control for DC microgrid with event-triggered signal transmissions," *IEEE Transactions on Sustainable Energy*, vol. 12, no. 3, pp. 1801-1810, Jul. 2021.

[24] L. Ding, Q. Han, L. Wang *et al*., "Distributed cooperative optimal control of DC microgrids with communication delays," *IEEE Transactions on Industrial Informatics*, vol. 14, no. 9, pp. 3924-3935, Sept. 2018.

[25] G. Chen and Z. Zhao, "Delay effects on consensus-based distributed economic dispatch algorithm in microgrid," *IEEE Transactions on Power Systems*, vol. 33, no. 1, pp. 602-612, Jan. 2018.

[26] M. Hamdi, M. Chaoui, L. Idoumghar *et al*., "Coordinated consensus for smart grid economic environmental power dispatch with dynamic communication network," *IET Generation, Transmission & Distribution*, vol. 12, no. 11, pp. 2603-2613, Apr. 2018.

[27] G. Wen, X. Yu, Z. Liu *et al*., "Adaptive consensus-based robust strategy for economic dispatch of smart grids subject to communication uncertainties," *IEEE Transactions on Industrial Informatics*, vol. 14, no. 6, pp. 2484-2496, Jun. 2018.

[28] J. Duan and M. Chow, "Robust consensus-based distributed energy man agement for microgrids with packet losses tolerance," *IEEE Transactions on Smart Grid*, vol. 11, no. 1, pp. 281-290, Jan. 2020.

[29] R. Wang, Q. Li, G. Li *et al*., "A gossip-based distributed algorithm for economic dispatch in smart grids with random communication link failures," *IEEE Transactions on Industrial Electronics*, vol. 67, no. 6, pp. 4635-4645, Jun. 2020.

[30] K. G. Murty and S. N. Kabadi, "Some NP-complete problems in quadratic and nonlinear programming," *Mathematical Programming*, vol. 39, no. 2, pp. 117-129, Mar. 1987.

[31] J. Zhao and F. Dörfler, "Distributed control and optimization in DC microgrids," *Automatica*, vol. 61, pp. 18-26, Nov. 2015.

[32] D. P. Bertsekas. *Constrained Optimization and Lagrange Multiplier Methods*. Nashua: Athena Scientific, 1996.

[33] D. P. Palomar and M. Chiang, "A tutorial on decomposition methods for network utility maximization," *IEEE Journal on Selected Areas in Communications*, vol. 24, no. 8, pp. 1439-1451, Jul. 2006.

[34] D. G. Luenberger. *Linear and Nonlinear Programming*, 4th ed. Berlin: Springer International Publishing, 2016.

[35] J. Xu, S. Zhu, Y. C. Soh *et al*., "Augmented distributed gradient methods for multi-agent optimization under uncoordinated constant stepsizes," in *Proceedings of 2015 54th IEEE Conference on Decision and Control (CDC)*, Osaka, Japan, Dec. 2015, pp. 2055-2060.

[36] M. Grant and S. Boyd. (Jan. 2014). CVX: MATLAB software for disciplined convex programming, version 2.1. [Online]. Available: http://cvxr.com/cvx

[37] E. Dallnese and A. Simonetto, "Optimal power flow pursuit," *IEEE Transactions on Smart Grid*, vol. 9, no. 2, pp. 942-952, Mar. 2018.

[38] X. Zhou, E. Dall'Anese, L. Chen *et al*., "An incentive-based online optimization framework for distribution grids," *IEEE Transactions on Automatic Control*, vol. 63, no. 7, pp. 2019-2031, Jul. 2018.

[39] A. Bernstein and E. Dall'Anese, "Real-time feedback-based optimization of distribution grids: a unified approach," *IEEE Transactions on Control of Network Systems*, vol. 6, no. 3, pp. 1197-1209, Sept. 2019.

[40] G. H. Golub and C. F. Loan, *Matrix Computations*. Baltimore: JHU Press, 2012.

[41] H. Robbins and D. Siegmund, "A convergence theorem for non negative almost supermartingales and some applications," in *Herbert Rob-*

bins Selected Papers. New York: Springer, 1985.
[42] M. Zhu and S. Martinez, "Discrete-time dynamic average consensus," *Automatica*, vol. 46, no. 2, pp. 322-329, Feb. 2010.
[43] A. Klenke. *Probability Theory*: *A Comprehensive Course*. New York: Springer Science & Business Media, 2007.
[44] A. Gut. *Probability*: *A Graduate Course*. New York: Springer Science & Business Media, 2005.

Jian Hu received the B.S.E.E degree from Southeast University, Nanjing, China, in 2012, and the Ph.D. degree in the College of Electrical Engineering, Zhejiang University, Hangzhou, China, in 2017. He is now working as an Engineer at Nanjing Power Supply Company, State Grid Corporation of China, Nanjing, China. His research interests include power electronics equipment, renewable energy, power quality, and operation and optimization of distribution network.

Hao Ma received the B.S., M.S., and Ph.D. degrees from Zhejiang University, Hangzhou, China, in 1991, 1994, and 1997, respectively, all in electrical engineering. Since 1997, he has been a Lecturer, Associate Professor, and Professor at Zhejiang University. From September 2007 to September 2008, he was a Delta Visiting Scholar at the North Carolina State University, Releigh, USA. He is the Vice Dean of the ZJU-UIUC Institute. He has authored two books and has authored or coauthored over 200 technical papers. He is currently the Director of Academic Committee of China Power Supply Society. He is the Associate Editor of the IEEE Journal of Emerging and Selected Topics in Power Electronics and the Journal of Power Electronics. He was the AdCom Member of the IEEE Industrial Electronics Society, the Technical Program Chair of the IEEE ISIE 2012, IEEE PEAC 2014 and IEEE PEAC 2018. His research interests include advanced control in power electronics, wireless power transfer, fault diagnosis of power electronic circuits and systems, and application of power electronics.